


RESEARCH

Open Access



# Rotman lens-based two-tier hybrid beamforming for wideband mmWave MIMO-OFDM system with beam squint

Bin Liu<sup>1,2</sup>  and Hongbo Zhu<sup>1\*</sup>

## Abstract

In this paper, we study the hybrid beamforming for the wideband mmWave multiuser MIMO-OFDM system. We characterize the frequency-dependent beam angle problem, i.e., beam squint effect. Firstly, we extend the mmWave channel model from the Saleh-Valenzuela representation with the consideration of beam squint. Secondly, a two-tier hybrid beamforming is proposed to achieve the maximum spectral efficiency in wideband mmWave multiuser MIMO-OFDM system. In the first tier, the Rotman lens array is adopted as the analog precoder to provide true-time-delay (TTD) and reduce the beam squint impairment. Moreover, the first-tier baseband precoder is designed based on block diagonalization (BD) to cancel inter-user interference. We further consider the finite spatial resolution and power leakage problem of the lens array. The second-tier hybrid precoder is proposed to collect the leak power with the phase shifter array. The optimal second-tier hybrid precoder design is formulated as the matrix factorization problem, and the two-tier hybrid precoding algorithm is based on the alternative minimization. It is found that both the beam squint and frequency-selective effect should be considered in the wideband mmWave system. Simulation results show that the proposed two-tier hybrid precoder could reduce beam squint impairment and inter-user interference, and could approximate to the optimal full-digital precoder with much fewer RF chains.

**Keywords:** Hybrid precoding, Millimeter wave, Wideband system, MIMO, Beam squint, Multiuser interference

## 1 Introduction

The capacity of the fifth generation (5G) wireless communication system is projected to bring 1000× increase to meet the data explosion by 2020 [1–5]. To achieve the ultra-reliable and available low-latency communications (uRLLC) for 5G/Beyond-5G (B5G) wireless system, more bandwidth, more advanced signal processing technologies, and together with cache techniques [6–8], are needed to guarantee the reliable and highly effective transmission. Millimeter wave emerges as the new radio in 5G communications to leverage the bandwidth shortage. Thanks to the shorter wave length, in mmWave massive multiple-input multiple-output (MIMO) system, more antennas can be packed within a relatively small physical dimension array to improve the spectral efficiency to compensate

the poor propagation characteristics of high-frequency channels [9–12].

However, for the conventional full-digital beamforming [13–15], each antenna in the array needs to be followed by a dedicated radio frequency (RF) chain, i.e., the number of RF chains is required to be the same with antennas. Unfortunately, though the full-digital could achieve the optimal performance, the high hardware cost makes it unaffordable for practical implementation, especially in such a large-scale array. To break through the hardware constraint of fully digital beamforming, hybrid analog/digital architectures were studied in [16–18]. By realizing the precoding process in both analog and digital domains, hybrid precoding could approximate the optimal precoder with fewer RF chains compared with the antennas scale. Exploiting the sparsity of the mmWave channel caused by high-frequency propagation loss, the authors in [16] proposed a low-complexity hybrid precoder based on orthogonal matching pursuit (OMP), which could approach the spectral efficiency of full-digital beamforming with much

\*Correspondence: [mliubin@hotmail.com](mailto:mliubin@hotmail.com)

<sup>1</sup>Jiangsu Key Laboratory of Wireless Communications, Nanjing University of Posts and Telecommunications, 210003 Nanjing, People's Republic of China  
Full list of author information is available at the end of the article

lower cost and power consumption. Two main hybrid precoder structures were investigated in [18], including fully connected hybrid architecture, i.e., each RF chain is connected to all the antennas through the phase shifter network, and partially connected hybrid architecture. The authors in [19] demonstrated that the hybrid beamforming performs almost as well as the full-digital beamforming in flat-fading channels on condition that the number of RF chains at the transceivers two times more than the number of data streams. Apart from the studies for the single-user MIMO system, the hybrid precoding for multiuser massive MIMO system was investigated in [20]. It is shown in [21] that the inter-user interference should be considered in the multiuser multicarrier system.

Limited works were involved in the hybrid beamforming for the wideband mmWave system, while the potential of mmWave communication that copes with uRLLC requirement in 5G/B5G lies in its ultra-wide bandwidth. Hybrid beamforming for the mmWave MIMO-OFDM system was investigated in [22–24]. Considering the frequency-selective channels, the authors in [22] designed the codebooks with limited channel state information (CSI), based on which optimal baseband precoders are obtained. In the OFDM-based system, the hybrid precoding was investigated in [23] for both single-user and multiuser system. The near-optimal closed-form solutions were given for fully connected and partially connected hybrid precoding in [24]. It further proposed the optimal subarrays partitioning/grouping strategy to maximize spectral efficiency. With partial channel angular information, the authors in [25] proposed hybrid precoding for the multiuser MIMO-OFDM system with frequency selectivity.

Though the frequency selectivity was considered, most of the aforementioned literature neglected the correlation of beam angle with signal frequency [26]. The frequency-dependent beam angle problem results from the difference of the additional transmission distance of each subcarrier signal arriving at different antennas in the array, which is called beam squint. The aforementioned work assumed that the additional transmission distances of signal arriving at different antennas were negligible. However, in massive MIMO systems, especially for mmWave communication with large bandwidth, the assumption under narrowband channel model may no longer be applicable [27–29]. The channel estimation in the wideband mmWave system with beam squint was investigated in [27], and further revealed dual-wideband effects in the angle domain and the delay domain. The delay Vandermonde matrix (DVM) algorithm was presented in [28] to reduce the beam squint effect with the low-complexity analog realizations. However, few works are observed in the hybrid beamforming for the wideband mmWave system with consideration of beam squint. It is found that the channel states of each subcarrier are quite different with

beam squint impairment, the limited number of RF chains in the hybrid structure constrains the degree of freedom to accommodate the difference of each subcarrier channel. The most straightforward approach is the full-digital realization. However, the high complexity and costs impede its practical implementation. It is a big challenge to design the low-complexity precoder in the wideband mmWave system.

## 2 Methods

In this paper, we study the hybrid beamforming for the wideband mmWave multiuser MIMO-OFDM system. Firstly, we characterize the frequency-dependent beam angle problem, i.e., beam squint effect, in the wideband mmWave system. Secondly, we extend the mmWave channel model with consideration of beam squint from the conventional mmWave Saleh-Valenzuela representation. Finally, the two-tier hybrid beamforming is proposed for the wideband mmWave multiuser MIMO-OFDM system. In the first tier, the Rotman lens array acts as the first-tier analog precoder to reduce the beam squint impairment by providing true-time-delay. Moreover, the first-tier baseband precoder is designed based on block diagonalization (BD) to cancel inter-user interference in the multiuser system. Considering the finite spatial resolution problem in practical lens array design, we proposed the second-tier hybrid precoder to collect the leak power with the phase shifter array. With the beam squint partial compensation and multiuser interference cancellation in the first-tier precoder, the optimal second-tier hybrid precoder design is formulated as the matrix factorization problem. Then, we develop the second-tier hybrid precoding algorithm based on the alternative minimization [18]. The main contributions of our work are summarized as follows:

- *Wideband mmWave channel model*: we characterize the beam squint effect in the wideband mmWave system and extend the mmWave channel model from Saleh-Valenzuela representation. It is found that beam squint effect and frequency selectivity should be considered in the wideband mmWave channel model.
- *Rotman lens-based two-tier hybrid beamforming*: we consider the hybrid beamforming for the wideband mmWave system with consideration of beam squint. Based on Rotman lens array, the two-tier hybrid beamforming proposed in this paper could reduce the beam squint impairment as well as multiuser interference in the multiuser mmWave MIMO-OFDM system.

The rest of the paper is organized as follows: we introduce the system model for the multiuser mmWave MIMO-OFDM system, and characterize wideband mmWave channel model with beam squint effect in

Section 2. The Rotman lens-based two-tier hybrid precoder is designed in Section 3. We evaluate the proposed algorithm, and exhibit the impact of beam squint and multi-user interference by the simulation results in Section 4. The conclusions are finally drawn in Section 5.

**Notations:** we introduce the notations used in this paper. A vector and a matrix are denoted by  $\mathbf{a}$  and  $\mathbf{A}$  separately, whose element on the  $i$ th row and  $j$ th column is  $\mathbf{A}_{i,j}$ ;  $(\cdot)^*$ ,  $(\cdot)^T$ ,  $(\cdot)^H$ ,  $(\cdot)^\dagger$  represent the conjugate, transpose, conjugate transpose, and Moore-Penrose pseudo inverse respectively; the trace is  $\text{Tr}(\cdot)$ ;  $|\cdot|$ ,  $\|\cdot\|_1$ ,  $\|\cdot\|_F$  and  $\|\cdot\|_\infty$  express the determinant, one Schatten norm, Frobenius norm, and infinite norm respectively.  $\angle \mathbf{A}$  denotes the argument of a complex matrix  $\mathbf{A}$ . Expectation is  $\mathbb{E}[\cdot]$ , and real part of a complex number is  $\Re[\cdot]$ . The Hadamard and Kronecker products are denoted by  $\circ$  and  $\otimes$  separately. The complex Gaussian distribution with mean  $\mathbf{x}$  and covariance matrix  $\mathbf{Y}$  is expressed as  $\mathcal{CN}(\mathbf{x}, \mathbf{Y})$ .

### 3 System model

In this section, we first characterize the beam squint effect in the wideband mmWave system. Then, we propose the Rotman lens-based true-time-delay (TTD) beamformer. With the consideration of finite spatial resolution constraint in practical lens array, we formulate the hybrid precoding problem.

#### 3.1 Wideband mmWave channel model

As shown in Fig. 1, we consider a signal from the far-field source impinging onto a uniform linear array (ULA) with azimuth angles of arrival and departure (AoAs and AoDs), where the ULA is with  $N$  identical and isotropic antennas, and the antennas are labeled as  $\{1, 2, \dots, N\}$ . The additional transition time by the distance of the signal traveled from the first antenna to the  $n$ th antenna is denoted by  $\Delta\tau_n$

$$\Delta\tau_n = \frac{(n-1)d \sin\theta}{c}, n \geq 1, \quad (1)$$

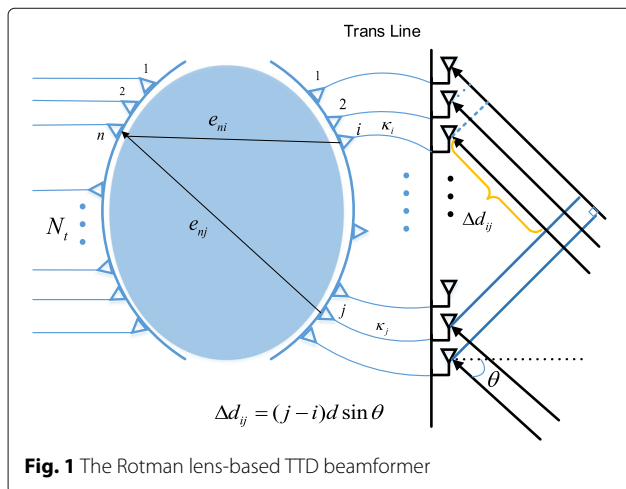


**Fig. 1** The Rotman lens-based TTD beamformer

where  $d$  is the array aperture,  $c$  is the velocity of light, and  $\Delta\tau_0 = 0$ . Consider the situation at receiver, and suppose the baseband signal arriving at the array is  $s(t)$ , the equivalent baseband signal received by the  $n$ th antenna is given by

$$y_n(t) = s(t - \Delta\tau_n) = s\left(t - \frac{(n-1)d \sin\theta}{c}\right). \quad (2)$$

Then, the received signal vector in time domain  $\mathbf{y}(t)$  is denoted by

$$\begin{aligned} \mathbf{y}(t) &= [y_0(t), y_1(t), \dots, y_{N-1}(t)]^T \\ &= [s(t - \Delta\tau_0), s(t - \Delta\tau_1), \dots, s(t - \Delta\tau_{N-1})]^T \\ &= \left[ s(t), s\left(t - \frac{d \sin\theta}{c}\right), \dots, s\left(t - \frac{(N-1)d \sin\theta}{c}\right) \right]^T, \end{aligned} \quad (3)$$

and the received signal vector in frequency domain  $\mathbf{y}(f)$  can be expressed as

$$\mathbf{y}(f) = \left[ s(f), s(f)e^{j2\pi f \frac{d \sin\theta}{c}}, \dots, s(f)e^{j2\pi f \frac{(N-1)d \sin\theta}{c}} \right]^T \quad (4)$$

$$= s(f) \left[ 1, e^{j\frac{2\pi}{\lambda} d \sin(\theta)}, \dots, e^{j\frac{2\pi}{\lambda} (N-1)d \sin(\theta)} \right]^T \quad (5)$$

$$= s(f)\mathbf{a}(\theta, f), \quad (6)$$

where  $\mathbf{a}(\theta, f)$  is the steering vector of the array, which is frequency-dependent, and can be written as

$$\mathbf{a}(\theta, f) = \frac{1}{\sqrt{N}} \left[ 1, e^{j\frac{2\pi}{\lambda} d \sin(\theta)}, \dots, e^{j(N-1)\frac{2\pi}{\lambda} d \sin(\theta)} \right]^T, \quad (7)$$

where  $\lambda$  is the wavelength of the signal. The array aperture  $d$  is often defined as the half wavelength  $d = \lambda/2$  in the aforementioned mmWave beamforming studies. Under this condition, the steering vector is independent of signal frequency, which can be given by [30]

$$\bar{\mathbf{a}}(\theta) = \frac{1}{\sqrt{N}} \left[ 1, e^{j\pi \sin(\theta)}, \dots, e^{j(N-1)\pi \sin(\theta)} \right]^T, \quad (8)$$

However, in practical system, the array aperture should be fixed and independent with the signal frequency and wavelength. As a matter of fact, constrained by the dynamic range of the transceiver, the arrays are usually designed based on the carrier frequency  $f_c$ . Typically, the aperture spacing  $d = \lambda_c/2$ , where  $\lambda_c = c/f_c$  is the wavelength of carrier. Though it is reasonable to approximate  $d = \lambda/2 \approx \lambda_c/2$  for the narrowband channel with the assumption that the bandwidth  $B$  satisfies the  $B \ll f_c$ , it is no more feasible in the wideband mmWave system.

Consider the spatial phase offset  $\Delta\varphi_n$  of  $n$ th antenna for signal with desired AoA/AoD  $\theta$ ,

$$\Delta\varphi_n = \frac{2\pi}{\lambda}(n-1)d \sin(\theta) = \pi(n-1)\delta \sin(\theta), \quad (9)$$

where  $\delta = f/f_c$ . The actual spatial AoA  $\hat{\theta}$  is

$$\hat{\theta}(f) = \arcsin(\delta \sin(\theta)). \quad (10)$$

It is observed that the AoA/AoD changes with the signal frequency, which is also called beam squint [31, 32] as shown in Fig. 2. The beam squint results in AoA/AoD diffusion, and broaden the beamwidth of the desired signal in the spatial domain. Moreover, the effect of beam squint is even magnified as the increase with the number of antennas and bandwidth in mmWave massive MIMO system. Most of the current work, however, ignore the beam squint effect, and assume that  $B \ll f_c$ , i.e.,  $\delta \approx 1$ , and the AoA/AoD is independent with the signal frequency, i.e.,  $\hat{\theta} \approx \theta$ . It is the basis of the aforementioned mmWave beamforming studies, but may not be applicable in the wideband system. It is of great importance to model the wideband mmWave channel, since the most fascination of millimeter wave in 5G communication is in its abundance spectrum and easy applying in the large-scale antenna array, which is expected to embrace the 1000× data rates increase [33–35].

In the following parts, we model the wideband mmWave channel with beam squint. First, the wideband steering vector is written as

$$\tilde{\mathbf{a}}(\theta, f) = \frac{1}{\sqrt{N}} \left[ 1, e^{j\pi \sin[\hat{\theta}(f)]}, \dots, e^{j(N-1)\pi \sin[\hat{\theta}(f)]} \right]^T, \quad (11)$$

which depends on the signal frequency. With high free-space path loss, the mmWave propagation environment is characterized by a clustered channel model [16, 22]. We extend the wideband clustered channel model based on the Saleh-Valenzuela representation. For the mmWave MIMO-OFDM system, the channel between

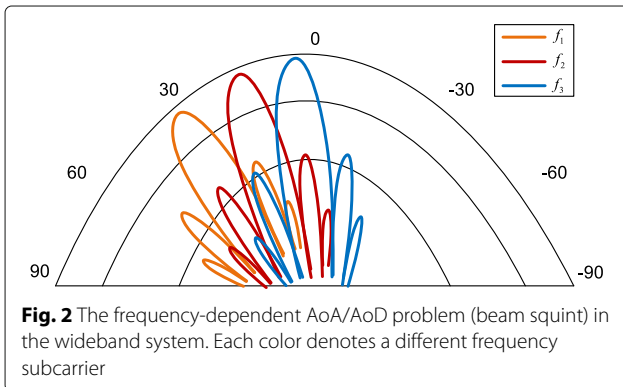


**Fig. 2** The frequency-dependent AoA/AoD problem (beam squint) in the wideband system. Each color denotes a different frequency subcarrier

the base station (BS) and  $u$ th user on  $k$ th subcarrier is depicted as

$$\begin{aligned} \mathbf{H}_u[k] &= \gamma_u \sum_{i=0}^{N_{cl,u}-1} \sum_{l=1}^{N_{ray,u}} \alpha_{il,u} \tilde{\mathbf{a}}_r(\theta_{il,u}^r, k) \tilde{\mathbf{a}}_t(\theta_{il,u}^t, k)^H e^{-j2\pi ik/K} \\ &= \gamma_u \sum_{i=0}^{N_{cl,u}-1} \sum_{l=1}^{N_{ray,u}} \alpha_{il,u} \mathbf{a}_r(\hat{\theta}_{il,u}^r[k]) \mathbf{a}_t(\hat{\theta}_{il,u}^t[k])^H e^{-j2\pi ik/K}, \end{aligned} \quad (12)$$

where the  $k \in \{0, 1, \dots, K-1\}$  is the subcarrier index,  $K$  is the total number of subcarriers.  $N_t$  and  $N_r$  are the transmit antenna of BS and receive antennas of  $u$ th user.  $N_{cl,u}$  and  $N_{ray,u}$  denote the number of clusters and the number of rays in each cluster.  $\alpha_{il,u}$  is the complex gain of  $l$ th ray in the  $i$ th clusters, and we assume all  $\alpha_{il,u}$  are independent and identically distributed (i.i.d.) random variables following the complex Gaussian distribution  $\mathcal{CN}(0, \sigma_{\alpha,i}^2)$  [6, 36, 37], and  $\sum_{i=1}^{N_{cl,u}} \sigma_{\alpha,i}^2 = \gamma_u$ , where  $\gamma_u = \sqrt{\rho_u N_t N_r / N_{cl,u} N_{ray,u}}$  is the normalization factor to satisfy  $\mathbb{E}[\|\mathbf{H}_{u,k}\|^2] = N_t N_r$ , and  $\rho_u$  is the path loss between the BS to the  $k$ th user.  $\tilde{\mathbf{a}}_r(\theta_{il,u}^r)$  and  $\tilde{\mathbf{a}}_t(\theta_{il,u}^t)$  represent the wideband steering vectors for desired azimuth angles of AoAs  $\theta_{il,u}^r$  and AoDs  $\theta_{il,u}^t$  for  $l$ th ray in the  $i$ th clusters respectively.

### 3.2 Rotman lens-based TTD beamformer

As discussed above, the beam squint, i.e., the frequency-dependent beam angle problem, results from the additional transition time (delay) of different antennas in the array. We rewrite the wideband mmWave channel as

$$\begin{aligned} \mathbf{H}_u[k] &= \gamma_u \sum_{i=0}^{N_{cl,u}-1} \sum_{l=1}^{N_{ray,u}} \alpha_{il,u} \tilde{\mathbf{a}}_r(\theta_{il,u}^r, k) \tilde{\mathbf{a}}_t(\theta_{il,u}^t, k)^H e^{-j2\pi ik/K} \\ &= \gamma_u \sum_{i=0}^{N_{cl,u}-1} \sum_{l=1}^{N_{ray,u}} \alpha_{il,u} (\tilde{\mathbf{a}}_r(\theta_{il,u}^r) \tilde{\mathbf{a}}_t(\theta_{il,u}^t)^H) e^{-j2\pi ik/K} \circ \Omega(\theta_{il,u}^t, \theta_{il,u}^r, k) \\ &= \tilde{\mathbf{H}}_u[k] \circ \Omega(\theta_{il,u}^t, \theta_{il,u}^r, k), \end{aligned} \quad (13)$$

where

$$\tilde{\mathbf{H}}_u[k] = \gamma_u \sum_{i=0}^{N_{cl,u}-1} \sum_{l=1}^{N_{ray,u}} \alpha_{il,u} (\tilde{\mathbf{a}}_r(\theta_{il,u}^r) \tilde{\mathbf{a}}_t(\theta_{il,u}^t)^H) e^{-j2\pi ik/K} \quad (14)$$

is the wideband mmWave channel without beam squint, which has been widely used based on discrete Fourier



transform (DFT) beamformer in [18, 22]. The beam squint could be solely characterized by  $\Omega(\theta_{il}^t, k)$ , an  $N_r \times N_t$  with whose  $(m, n)$ th element

$$[\Omega(\theta_{il}^t, \theta_{il}^r, k)]_{m,n} \triangleq \exp\left(-j2\pi dBk/K \cdot \frac{m \sin(\theta_{il}^t) + n \sin(\theta_{il}^r)}{c}\right), \quad (15)$$

which denotes the additional delay of  $m$ th and  $n$ th antenna with reference antennas (0th) in the receiver and transmitter respectively, where  $m \in \{1, 2, \dots, N_r\}$  and  $n \in \{1, 2, \dots, N_t\}$ . The effect of beam squint will be increasingly distinct with the antenna scale and total bandwidth. By the hardware constraint by the conventional DFT-based beamformer with phase shifter array, efficiency, and reliability cannot be guaranteed. It is mainly by the fact that the delay of different antennas depends on the angle (AoA/AoD) and the frequency of the signal as shown in (1), and cannot be dynamically compensated by the DFT-based beamformer, especially for the wideband system.

The true-time-delay beamformer is attractive for the future wideband systems, which could provide the accurate delay caused by the beam squint effect. Among various TTD beamformers, the Rotman lens is broadband with simple realization structure. Owing its low-complexity structure, it could be fabricated with printed circuit boards [38]. In this paper, we study the full-connected hybrid beamforming with the Rotman lens-based RF analog precoder to reduce the beam squint effect in the wideband mmWave system. Let us show the principle of true-time-delay in Rotman lens.

We show the schematic representation of Rotman lens [38, 39] in Fig. 1, where  $N$  beam ports are on the left side of the lens array (i.e., beam-port contour) with the  $N$  antenna ports on the left side (i.e., antenna-port contour). The distance of wave transmission paths from the  $i$ th and  $j$ th antenna ports to the  $n$ th beam port separately write as  $z_{ni} = e_{ni} + \kappa_i$  and  $z_{nj} = e_{nj} + \kappa_j$ , where the length of transmission line is represented by  $\kappa$  with its subscript  $i$  denoting the numerical order of antenna. The  $e_{ni}$  and  $e_{nj}$  are the transmission lengths from the  $i$ th and  $j$ th antenna to the  $n$ th beam port in the Rotman lens. The additional transmission delay distance of the signal that travels from the  $i$ th antenna to the  $j$ th antenna is  $\Delta d_{ij} = (j - i)d \sin(\theta)$ . The design target of Rotman lens-based TTD beamformer is to shape its geometric shape, including beam-port and antenna-port contours, to satisfy the following equation [38]

$$z_{ni} - z_{nj} = \Delta d_{ij}. \quad (16)$$

With the principle of TTD in Rotman lens, we further characterize its function into the mathematical model. At

the transmitter side, considering the Rotman lens as a multiple-ports network, it could be depicted by a  $N_t \times N_t$  matrix  $\mathbf{P}_{\text{RM}}$ . The electromagnetic gathering of lens array is usually modeled as a DFT matrix with  $N_t$  orthogonal steering vectors, i.e.,

$$\mathbf{P}_{\text{RM}} = [\mathbf{b}_{N_t}(\bar{\theta}_1), \mathbf{b}_{N_t}(\bar{\theta}_2), \dots, \mathbf{b}_{N_t}(\bar{\theta}_{N_t})], \quad (17)$$

where the spatial directions  $\bar{\theta}_i = \frac{1}{N_t} \left(i - \frac{N_t+1}{2}\right)$ ,  $i = 1, 2, \dots, N_t$ , and  $\mathbf{b}_N(\bar{\theta})$  represent the steering vector for the spatial direction  $\theta$ ,

$$\mathbf{b}_N(\theta) = \left[1, e^{j\frac{2\pi}{\lambda c} d \sin(\theta)}, \dots, e^{j\frac{2\pi}{\lambda c} (N-1) d \sin(\theta)}\right]^T. \quad (18)$$

As the beam-port and antenna-port contours, transmission line length is designed to compensate the additional phase offset by the beam squint effect, the true-time-delay in full-array Rotman lens beamformer could be further modeled as a matrix  $\Theta(\theta_{il}^t, k)$  whose element satisfies

$$[\Theta(\theta_{il}^t, k)]_{ij} = \exp\left(j2\pi ijBk/K \cdot \frac{d \sin(\bar{\theta}_{il}^t)}{c}\right), \quad (19)$$

where  $\bar{\theta} \in \{0, 2\pi/M, \dots, 2\pi(M-1)/M\}$  and  $M$  is the number of beam ports. The finite angular resolution  $\Delta\theta = 2\pi/M$  and the  $\bar{\theta} = \theta + \Delta\theta$ . In practical, it is hard to design the Rotman lens strictly according to (16) that is feasible for all signals with various and continuous directions. Actually, it is often the case that we consider the finite angular of the signal to design the TTD transmission lines. When the  $\Delta\theta \rightarrow 0$ , it is found that the TTD function in Rotman lens could remove the beam squint impairment by making up the accurate extra phase offset, i.e.,  $\Theta(\bar{\theta}_{il}^t, k) \rightarrow \Theta(\theta_{il}^t, k) = \Omega(\theta_{il}^t, k)^*$ . Then, the equivalent channel after the signal passing through the Rotman lens beamformer at both sides is written as

$$\begin{aligned} & \hat{\mathbf{H}}_u[k] \\ &= \mathbf{P}_{\text{RM}} \bar{\mathbf{H}}_u[k] \circ \Omega(\theta_{il}^t, \theta_{il}^r, k) \circ \Theta(\theta_{il}^t, k) \circ \Theta(\theta_{il}^r, k) \\ &\rightarrow \mathbf{P}_{\text{RM}} \bar{\mathbf{H}}_u[k], \end{aligned} \quad (20)$$

and  $\hat{\mathbf{H}} = [\hat{\mathbf{H}}_1, \dots, \hat{\mathbf{H}}_u, \dots, \hat{\mathbf{H}}_U]$ , where  $\hat{\mathbf{H}}_u = [\hat{\mathbf{H}}_u[1], \dots, \hat{\mathbf{H}}_u[k], \dots, \hat{\mathbf{H}}_u[K]]$ . It observed that the ideal Rotman lens-based TTD beamformer could remove the beam squint matrix and perform spatial discrete fourier transform to the channel.

### 3.3 Power leakage in finite-resolution lens array

In fact, it is impossible to simultaneously design all beam ports in Rotman lens strictly according to (16). Moreover, in practical lens array, the spatial resolution in the lens array is limited, and there are only infinite and discrete beam port (focal point) in the focal point arc, while

the AoA/AoD are continuously distributed in the spatial domain. The actual angle of one path cannot find the matched beam port at the lens antenna array. It nevertheless results in the power leakage [40], i.e., the power of one path will leak into multiple beams. From Lemma 1 in [40], for the worst case, i.e., the single path in one cluster, where  $N_{cl,u} = 1$  and  $N_{ray,u} = 1$ , if we select only one beam with the highest power, the ratio  $\eta$  of the leaked power to the total power is

$$\eta = 1 - \frac{1}{2 \sum_{i=1}^{N/2} \frac{\sin^2(\pi/2N)}{\sin^2((2i-1)\pi/2N)}} \quad (21)$$

It is found that the power leakage ratio  $\eta \approx 0.5947$  when the antenna  $N_t = 128$ . Over half of power is lost if only one beam is selected for one path in the finite resolution Rotman lens array. The practical way to design Rotman lens is usually to pick up multiple focal points to collect the leakage power [38, 39]. Most of these works choose the full-digital method to collect the multiple beams, for example, the same number of RF chain is required to collect multiple beams. Though more power it may collect, it inevitably incur higher hardware complexity and energy consumption [41, 42]. To this end, we propose to adopt a phase shifter array as the second-tier analog RF precoder, which could collect multiple beams of one path through one RF chain [40]. More specifically, each RF chain could connect to all the beam ports  $N_t$  through the  $N_t$  phase shifters. The number of RF chain to collect multiple beams is  $N_{RF}$  is much smaller than the antenna  $N_{RF} < N_t$ .

### 3.4 Problem formulation

As shown in Fig. 3, we study the downlink transmission of a mmWave multiuser MIMO-OFDM system, where the full-connected hybrid structure is adopted at both sides. The base station (BS) has  $N_t$  antennas.  $N_s$  data streams are delivered to total  $U$  users, and each user is equipped with  $N_r$ . There are only limited RF chains  $N_{RF}^t$  and  $N_{RF}^r$  for

the BS and each user, and satisfy the constraints  $UN_s \leq N_{RF}^t \leq N_t$  and  $N_s \leq N_{RF}^r \leq N_r$ . In this paper, we consider that the Rotman lens array is only used in the BS side, and only the ULA array and phase shifter network are used in the user side. As it is often the case that  $N_t \gg N_r$  in multiuser MIMO system, the beam squint effect in user side is negligible comparing with the base station. With reciprocity of downlink and uplink channel, we also could compensate the beam squint of both sides in the BS with the Rotman lens array. Thus, we have the  $u$ th ( $1 \leq u \leq U$ ) user's received signal over the  $k$ th subcarrier as

$$\begin{aligned} \mathbf{y}_u[k] = & \mathbf{W}_{BB,u}^H[k] \mathbf{W}_{RF}^H \hat{\mathbf{H}}_u[k] \cdot \left( \sum_{\mu=1}^U \mathbf{F}_{RF} \mathbf{F}_{BB,\mu}[k] \mathbf{s}_\mu[k] \right) \\ & + \mathbf{W}_{RF}^H \mathbf{W}_{BB,u}^H[k] \mathbf{n}_u[k], \end{aligned} \quad (22)$$

where  $\mathbf{s}_\mu[k] \in \mathbb{C}^{N_s}$  is the transmitted symbol vector for the  $u$ th user over the  $k$ th subcarrier that satisfies  $\mathbb{E}[\mathbf{s}_\mu[k] \mathbf{s}_\mu^H[k]] = \frac{1}{KUN_s} \mathbf{I}_{N_s}$ , the digital baseband precoders and combiners are denoted by  $\mathbf{F}_{BB,\mu}[k] \in \mathbb{C}^{N_{RF}^t \times N_s}$  and  $\mathbf{W}_{BB,\mu}[k] \in \mathbb{C}^{N_{RF}^r \times N_s}$ , respectively. Since the analog precoding is a post-IFFT processing, all the users and subcarriers share one common second-tier analog precoder  $\mathbf{F}_{RF} \in \mathbb{C}^{N_t \times N_{RF}^t}$  and combiner  $\mathbf{W}_{RF} \in \mathbb{C}^{N_r \times N_{RF}^r}$  [18].  $\mathbf{n}_u[k] \in \mathbb{C}^{N_r}$  denotes the additive noise at the  $u$ th user, whose element follow i.i.d  $\mathcal{CN}(0, \sigma^2)$ . As shown in [16, 18], the design of precoders and combiners have similar mathematical process. Therefore, we will separate the precoders and combiners design, and mainly focus on the optimal precoder design in the following. The process can be easily applied for combiners. Note that, the combiner could be deemed as the special case when the beam squint is removed. It is found in [16] that the optimal hybrid precoders design could be approximated by minimizing the

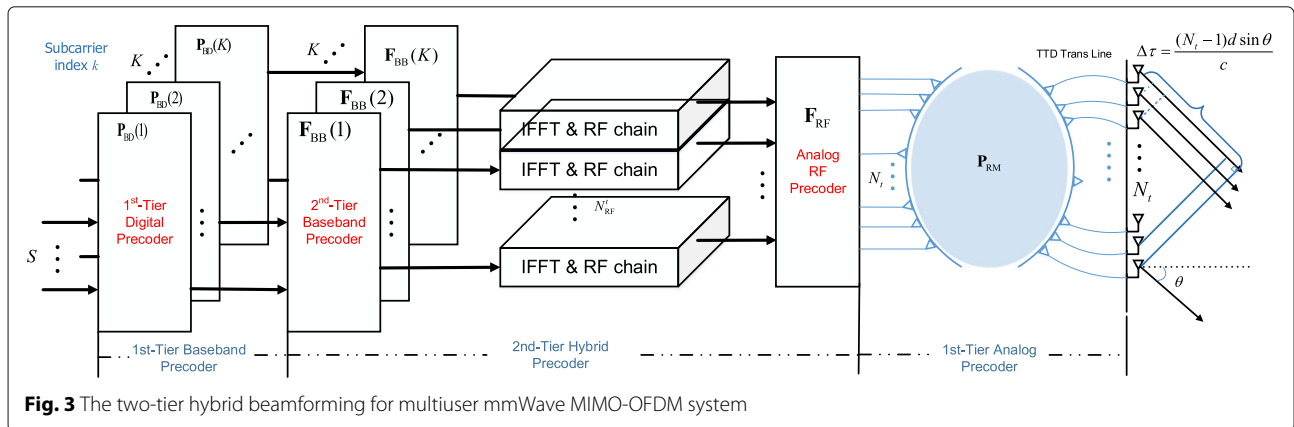


**Fig. 3** The two-tier hybrid beamforming for multiuser mmWave MIMO-OFDM system

Euclidean distance between the unconstrained digital precoder  $\mathbf{F}_{\text{opt}}$  and the hybrid precoder. Thus, the second-tier hybrid precoder design problem could be formulated as

$$\begin{aligned} (\mathbf{F}_{\text{RF}}^{\text{opt}}, \mathbf{F}_{\text{BB}}^{\text{opt}}) &= \arg \min_{\mathbf{F}_{\text{RF}}, \mathbf{F}_{\text{BB}}} \|\mathbf{F}_{\text{opt}} - \mathbf{F}_{\text{RF}} \mathbf{F}_{\text{BB}}\|_F \\ \text{s.t. } & |(\mathbf{F}_{\text{RF}})_{i,j}| = 1 \\ & \|\mathbf{F}_{\text{RF}} \mathbf{F}_{\text{BB}}\|_F^2 = KUN_s, \end{aligned} \quad (23)$$

where  $\mathbf{F}_{\text{opt}} = [\mathbf{F}_{\text{opt},1}[1], \dots, \mathbf{F}_{\text{opt},u}[k], \dots, \mathbf{F}_{\text{opt},U}[K]]$ , and  $\mathbf{F}_{\text{opt},u}[k]$  is the unconstrained digital precoder for the equivalent channel between the Rotman lens array and the user  $\hat{\mathbf{H}}_u[k] = \mathbf{P}_{\text{RM}} \bar{\mathbf{H}}_u[k]$ . The baseband precoder is  $\mathbf{F}_{\text{BB}} \in \mathbb{C}^{N_{\text{RF}}^t \times KUN_s}$ , and  $\mathbf{F}_{\text{BB}} = [\mathbf{F}_{\text{BB},1}[1], \dots, \mathbf{F}_{\text{BB},u}[k], \dots, \mathbf{F}_{\text{BB},U}[K]]$ . The unit modulus constraints by the analog precoders are implemented with phase shifters, where only the phases of the signals are adjustable and the second constraint is by the transmit power constraint at the BS side.

#### 4 Two-tier multiuser hybrid precoder design

The first-tier analog precoder is the Rotman lens array-based beamformer, which is designed to compensate the beam squint impairment in the wideband mmWave system. We also choose block diagonalization (BD)-based digital precoder in the first tier to reduce the inter-user interference. In the following, we illustrate the process of the two-tier hybrid precoder design. Firstly, we consider the practical problem of low-resolution lens array and develop the second-tier precoder to solve the power leakage problem that caused imperfect lens array in the first-tier analog precoder. To reduce the hardware cost and energy consumption, we propose second-tier hybrid precoder based on phase shifter network. Secondly, with the equivalent channel, the optimal second-tier hybrid precoders design is formulated as a matrix decomposition problem in (23). We try to find the accurate approximation hybrid precoder that minimizes the Euclidean distance with  $\mathbf{F}_{\text{opt}}$ . Finally, we complete the design of the first-tier baseband precoder based on block diagonalization precoding.

##### 4.1 The second-tier hybrid precoder design

Due to the complication in jointly optimizing these two matrices in (23), we decouple second-tier analog and baseband precoder design, and adopt the alternating minimization method [18] to find the optimal results. According to the principle of alternating minimization, only one part of hybrid precoder is optimized in each step with the assumption that other parts are fixed. Herein, we temporarily consider the optimal digital precoders without

the power constraint in (23), and the precoders will be normalized in the last step to satisfy power constraint, i.e.,

$$\begin{aligned} \min_{\mathbf{F}_{\text{RF}}, \mathbf{F}_{\text{BB}}} & \|\mathbf{F}_{\text{opt}} - \mathbf{F}_{\text{RF}} \mathbf{F}_{\text{BB}}\|_F \\ \text{s.t. } & |(\mathbf{F}_{\text{RF}})_{i,j}| = 1 \end{aligned} \quad (24)$$

The problem is intrinsically non-convex with the unit modulus constraints. Though manifold optimization could directly address the unit modulus constraints and give near-optimal solution of the problem [18], it nevertheless incurs high computational complexity, especially for the large-scale antenna array. It is found that computational complexity could be largely reduced if the baseband precoder satisfies the semi-orthogonal property. It is noticed that the columns of the unconstrained optimal precoding matrix  $\mathbf{F}_{\text{opt}}$  should be mutually orthogonal in order to mitigate the multiplexed streams interference [18, 43–45]. Besides, the additional orthogonal assumption of the digital precoder enable to directly extract the phases of the analog precoder from the of an equivalent precoder determined by the digital precoder and the unconstrained optimal digital precoder  $\mathbf{F}_{\text{opt}}$ , and only results in negligible loss [18]. Thus, we have the semi-orthogonal property of baseband precoder as

$$\mathbf{F}_{\text{BB}} \mathbf{F}_{\text{BB}}^H = \beta \mathbf{G} \beta \mathbf{G}^H = \beta^2 \mathbf{I}_{N_{\text{RF}}^t}, \quad (25)$$

where  $\mathbf{G}$  is a same dimension matrix with  $\mathbf{F}_{\text{BB}}$ . It is observed that the interest of introducing orthogonal property is to enable the  $\mathbf{F}_{\text{RF}}$  to remove the product form with  $\mathbf{F}_{\text{BB}}$ , and the details can be found in [18]. With the semi-orthogonal property, the problem (24) is rewritten as

$$\begin{aligned} \min_{\mathbf{F}_{\text{RF}}, \mathbf{G}} & \|\mathbf{F}_{\text{opt}} \mathbf{G}^H - \mathbf{F}_{\text{RF}}\|_F^2 \\ \text{s.t. } & \begin{cases} |(\mathbf{F}_{\text{RF}})_{i,j}| = 1, \forall i, j \\ \mathbf{G} \mathbf{G}^H = \mathbf{I}_{N_{\text{RF}}^t}. \end{cases} \end{aligned} \quad (26)$$

*Proof* See Appendix A.  $\square$

The analog precoder  $\mathbf{F}_{\text{RF}}$  has closed-form solution as

$$\mathbf{F}_{\text{RF}} = \exp \{j \angle (\mathbf{F}_{\text{opt}} \mathbf{G}^H)\}. \quad (27)$$

It is observed that the phases of  $\mathbf{F}_{\text{RF}}$  can be extracted from the phases of  $\mathbf{F}_{\text{opt}} \mathbf{G}^H$ . Thus, the closed-form solution is produced from the Euclidean projection  $\mathbf{F}_{\text{opt}} \mathbf{G}^H$  on the feasible set of analog precoder  $\mathbf{F}_{\text{RF}}$ .

From (26), it implies the design of baseband precoder is equivalent to find the unitary precoding matrix  $\mathbf{G}$ , and then find corresponding precoding matrix  $\mathbf{F}_{\text{BB}}$ . It forms a typical semi-orthogonal Procrustes problem (OPP) [18].

With fixed  $\mathbf{F}_{\text{RF}}$  from (27), we design the baseband precoder by solving the optimization problem as follows:

$$\begin{aligned} \min_{\mathbf{G}} \quad & \|\mathbf{F}_{\text{opt}}\mathbf{G}^H - \mathbf{F}_{\text{RF}}\|_F^2 \\ \text{s.t.} \quad & \mathbf{G}\mathbf{G}^H = \mathbf{I}_{N_{\text{RF}}^t}. \end{aligned} \quad (28)$$

From (34), (28) is equivalent to solve the optimization problem

$$\begin{aligned} \max_{\mathbf{G}} \quad & \Re\text{Tr}\left(\mathbf{G}\mathbf{F}_{\text{opt}}^H\mathbf{F}_{\text{RF}}\right) \\ \text{s.t.} \quad & \mathbf{G}\mathbf{G}^H = \mathbf{I}_{N_{\text{RF}}^t}. \end{aligned} \quad (29)$$

By the dual norm property, the objective function has

$$\begin{aligned} \Re\text{Tr}\left(\mathbf{G}\mathbf{F}_{\text{opt}}^H\mathbf{F}_{\text{RF}}\right) & \leq \left|\text{Tr}\left(\mathbf{G}\mathbf{F}_{\text{opt}}^H\mathbf{F}_{\text{RF}}\right)\right| \\ & \stackrel{(a)}{\leq} \|\mathbf{G}^H\|_{\infty} \cdot \|\mathbf{F}_{\text{opt}}^H\mathbf{F}_{\text{RF}}\|_1 \\ & = \|\mathbf{F}_{\text{opt}}^H\mathbf{F}_{\text{RF}}\|_1 \\ & = \sum_{i=1}^{N_{\text{RF}}^t} \sigma_i, \end{aligned} \quad (30)$$

where (a) is by the Hölder's inequality, and it holds only when

$$\mathbf{G} = \mathbf{V}\mathbf{U}_1^H, \quad (31)$$

where  $\mathbf{U}_1\mathbf{S}\mathbf{V}^H = \mathbf{F}_{\text{opt}}^H\mathbf{F}_{\text{RF}}$  is the SVD of  $\mathbf{F}_{\text{opt}}^H\mathbf{F}_{\text{RF}}$ , and  $\mathbf{S}$  is a diagonal matrix with first non-zero  $N_{\text{RF}}^t$  singular values  $\sigma_1, \dots, \sigma_{N_{\text{RF}}^t}$ .

#### 4.2 Block diagonalization baseband precoder design

As aiming to collect the power leakage only by approximating the unconstrained digital  $\mathbf{F}_{\text{opt}}$ , the second-tier hybrid precoder can hardly cancel the inter-user interference. It is found in [21, 46, 47] that the residual inter-user interference in hybrid beamforming is serious, and usually results in dramatic performance loss in the hybrid precoding, especially at high SNR regimes. More importantly, in the multiuser multicarrier wideband systems, the second-tier analog precoder  $\mathbf{F}_{\text{RF}}$  is commonly shared by a large number of users and subcarriers, which further degrade the performance. To this end, we design the extra baseband precoder  $\mathbf{P}_{\text{BD}}$  in the first tier based on block diagonalization (BD) precoder [48] in this subsection.

With Rotman lens array-based analog precoder (first tier), and second-tier hybrid precoder and combiner, we define the effective channel for  $u$ th user on  $k$ th subcarrier as

$$\check{\mathbf{H}}_u[k] \triangleq \mathbf{W}_{\text{BB},u}^H[k] \mathbf{W}_{\text{RF}}^H \hat{\mathbf{H}}_u[k] \mathbf{F}_{\text{RF}} \mathbf{F}_{\text{BB}}[k], \quad (32)$$

where  $\hat{\mathbf{H}}_u[k]$  is the equivalent channel with Rotman lens array compensating the beam squint.  $\mathbf{F}_{\text{BB}}[k] =$

$[\mathbf{F}_{\text{BB},1}[k], \dots, \mathbf{F}_{\text{BB},u}[k], \dots, \mathbf{F}_{\text{BB},U}[k]] \in \mathbb{C}^{N_{\text{RF}}^t \times UN_s}$  is the digital precoder on the  $k$ th subcarrier, and  $\check{\mathbf{H}}_u[k] \in \mathbb{C}^{N_s \times UN_s}$ . With principle of BD, the first-tier baseband precoder  $\mathbf{P}_{\text{BD}}$  satisfies

$$\check{\mathbf{H}}_i[k] \mathbf{P}_{\text{BD},u}[k] = 0, \quad u \neq i. \quad (33)$$

More details can be found in [48]. To summarize, the first-tier analog precoder is based on Rotman lens array and could remove the beam squint in the wideband system. After the first-tier analog precoder, it produce the squint-free equivalent channel  $\hat{\mathbf{H}}$ , and design the second-tier hybrid precoder to solve the power leakage problem caused by finite spatial resolution of lens antenna array. Moreover, the first-tier baseband precoder  $\mathbf{P}_{\text{BD}}$  is proposed to cancel the inter-user interference. Based on the closed-form solutions for the second-tier hybrid precoders and BD precoder, we summarize the two-tier hybrid precoding algorithm in Algorithm 1.

---

#### Algorithm 1 Two-tier hybrid precoding algorithm

---

- 1: **Input:**  $\mathbf{F}_{\text{opt}}$
  - 2: Initialize  $\mathbf{F}_{\text{RF}}^{(0)}$  with random phase and set  $i = 0$
  - 3: **repeat:**
  - 4: Fix  $\mathbf{F}_{\text{RF}}^{(i)}$  and calculate SVD decomposition:  $\mathbf{F}_{\text{opt}}^H \mathbf{F}_{\text{RF}}^{(i)} = \mathbf{U}_1^{(i)} \mathbf{S}^{(i)} \mathbf{V}^{(i)H}$ ;
  - 5:  $\mathbf{G}^{(i)} = \mathbf{U}_1^{(i)} \mathbf{V}^{(i)H}$ ;
  - 6: Fix  $\mathbf{F}_{\text{BB}}^{(i)}$  and update  $\mathbf{F}_{\text{RF}}$  according to (27):  $\mathbf{F}_{\text{RF}}^{(i+1)} = \exp\{j\angle(\mathbf{F}_{\text{opt}}\mathbf{G}^{(i)H})\}$ ;
  - 7:  $i \leftarrow i + 1$ ;
  - 8: **until:** the stopping conditions;
  - 9: Calculate the effective channels  $\check{\mathbf{H}}_i[k]$  in (32);
  - 10: Obtain first-tier baseband precoder  $\mathbf{P}_{\text{BD},u}[k]$  according to (33);
  - 11: Combine the two-tier's baseband precoders  $\mathbf{P}_{B,u}[k] = \mathbf{F}_{\text{BB},u}[k] \mathbf{P}_{\text{BD},u}[k]$ ;
  - 12: Power constrain normalization (23):  $\bar{\mathbf{P}}_B = \frac{\sqrt{KUN_s}}{\|\mathbf{F}_{\text{RF}}\mathbf{P}_B\|_F} \mathbf{P}_B$ .
- 

## 5 Numerical results

In this section, we will evaluate the proposed two-tier hybrid precoder by comparing with other mmWave precoding schemes. The impacts of beam squint effect in the wideband system, as well as multiuser interference in the hybrid architecture MIMO-OFDM system on beamforming performance, are investigated. We generate the wideband channel model based on Saleh-Valenzuela representation with the angle of AoDs and AoAs following Laplacian distribution with mean angles within  $[0, 2\pi)$ , and the angular spread is assumed as  $10^\circ$ . The antenna



aperture in ULA is a half wavelength of the carrier frequency  $d = \lambda_c/2$ . All the simulation results are averaged over 5000 channel realizations.

### 5.1 The effect of beam squint

To exhibit the beam squint effect, we compare the spectral efficiency and bit error rate (BER) with the state-of-the-art precoding schemes in the single-user MIMO-OFDM system with  $N_t = 256$  and  $N_r = 64$  at transmitter and receiver separately. The total bandwidth  $B = 1.2$  GHz and carrier frequency  $f_c = 60$  GHz. We consider the worst case when the number of RF chains is equal to that of the data streams, i.e.,  $N_{RF}^t = N_{RF}^r = N_s = 4$ .

As shown in Fig. 4, two benchmark schemes are selected for comparing the spectral efficiency performance: (1) optimal digital TDD precoder scheme is a full-digital architecture, where each antenna is followed by an individual RF chain. Since with the true-time-delay function and the large numbers of RF chain, it is the upper bound of precoder design. (2) OMP-based hybrid precoder: orthogonal matching pursuit (OMP) algorithm [16] is commonly used to obtain the optimal analog and digital precoder in hybrid precoding architecture. The OMP is a kind of one-tier hybrid precoder with phase shifter network. It is observed in Fig. 4 that the proposed two-tier hybrid precoder scheme could approach the optimal digital precoder. In the proposed two-tier hybrid precoder, the Rotman lens-based TTD precoder act the first tier. It provides the approximate true-time-delay and compensates the beam squint effect. After that, with phase

array, the second-tier hybrid precoder could collect the power leakage caused by the finite spatial resolution in the practical lens array. The alternation minimization in the second-tier precoder could well approach the full-digital architecture with much fewer RF chains, which are quite energy-hungry.

It is shown in Fig. 4 that there a gap between the OMP-based hybrid precoder with other schemes. The reason is that the OMP-based hybrid precoder is actually a kind one-tier DFT beamformer and cannot provide true-time-delay. The original feasible searching space of analog precoders  $\mathbf{F}_{RF}$  in OMP algorithm [16] locates in the set of steering vectors  $\tilde{\mathbf{a}}_r(\theta_{il}^r, k)$  and  $\tilde{\mathbf{a}}_t(\theta_{il}^t, k)$ , which is frequency-dependent. As shown in Section 2, the analog precoder design is a post-IFFT process, and  $\mathbf{F}_{RF}$  is commonly used for all users over various frequency bands, i.e.,  $\mathbf{F}_{RF}$  is frequency-independent. As a matter of fact, without considering beam squint, the hybrid precoder in the OMP algorithm is designed only according to the carrier frequency  $f_c$ . However, the channel states of each subcarrier are quite different with beam squint impairment, the limited number of RF chains in one-tier DFT hybrid structure constrains the degree of freedom to accommodate the difference of each subcarrier channel. A larger gap will be easily observed with the increase of the fractional bandwidth  $B/f_c$ .

To further demonstrate the beam squint effect, we plot the BER performance versus symbol SNR for four precoder schemes in Fig. 5. The digital DFT precoder and the hybrid DFT precoder are designed based on

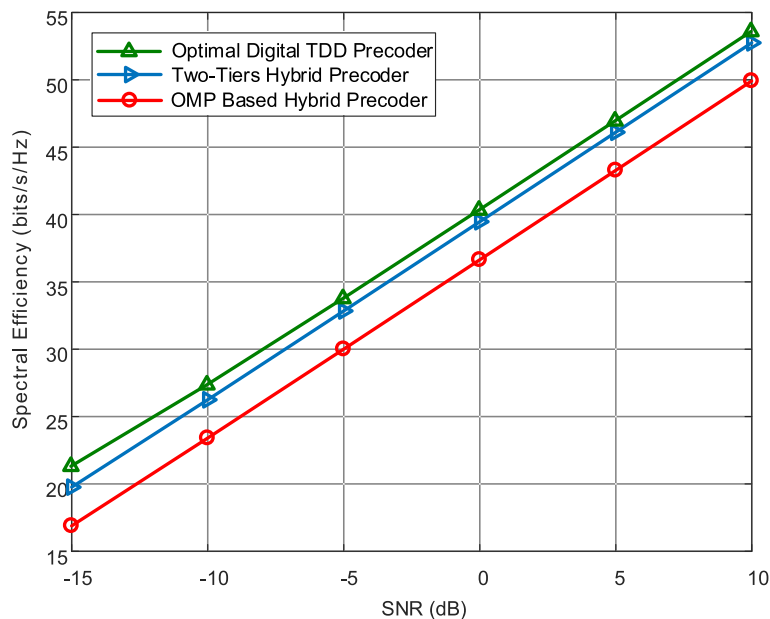


**Fig. 4** Spectral efficiency achieved by different precoding schemes in single-user mmWave MIMO-OFDM systems with  $N_t = 256$ ,  $N_r = 64$ , total bandwidth  $B = 1.2$  GHz,  $f_c = 60$  GHz,  $N_{RF}^t = N_{RF}^r = N_s = 4$

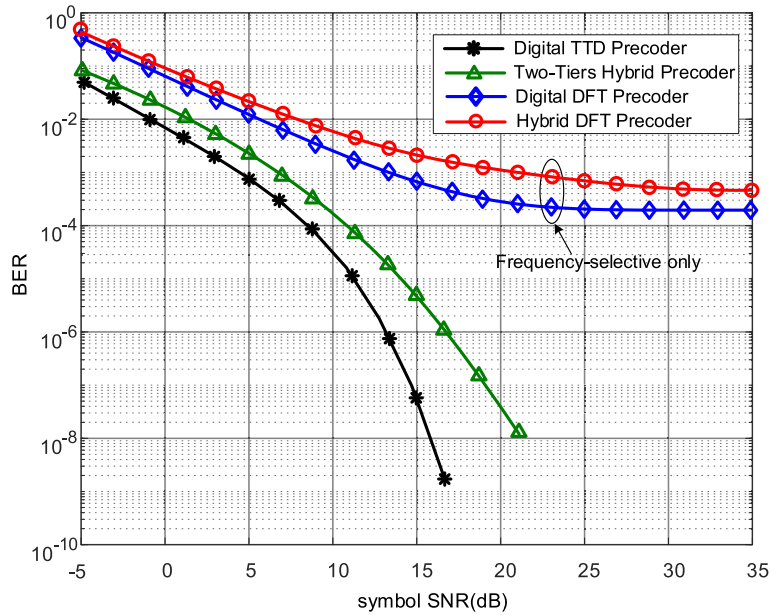


**Fig. 5** BER performance comparison in single-user mmWave MIMO-OFDM systems with  $N_t = 256$ ,  $N_r = 64$ , total bandwidth  $B = 1.2$  GHz,  $f_c = 60$  GHz,  $N_{\text{RF}}^t = N_{\text{RF}}^r = N_s = 4$

conventional mmWave MIMO-OFDM channel model, which only considers the frequency-selective channel and neglects the beam squint effect. As observed in Fig. 5, there are error floors in two DFT precoders. Owing to frequency-dependent beam angle problem in beam squint, the orthogonality condition in angular domain is not satisfied any more, especially when the number of antennas and subcarriers is finite [27]. The damage of orthogonality results in this error floor. To summarize, the beam squint cannot be ignored in the wideband mmWave channel if there is no true-time-delay compensation. Notice that, though with large number of RF chains as DFT digital precoder is, it only considers the frequency selectivity in multi-carriers system, and does not provide the true-time-delay since it neglects the beam squint in its design process. The digital TTD precoder and the proposed hybrid precoder are designed with the consideration of beam squint and could provide true-time-delay, which appeals to better BER performance. Constrained the imperfection of Rotman lens-based TTD precoder, i.e., the angular resolution  $\Delta\theta \neq 0$ , and the difference in optimal precoder matrix factorization and approximation, we can observe a narrow gap between the proposed two-tier hybrid precoder with digital TTD precoder. We thus obtain the insights that the BER error floors were observed if only considering the frequency selectivity in the wideband channel model, and both the frequency selectivity and beam squint effect should be considered in the wideband mmWave system.

## 5.2 Multiuser system

In this subsection, we present the comparison of proposed hybrid precoder with optimal digital precoder with optimal digital precoder and one-tier hybrid precoder in multiuser MIMO-OFDM system, where the BS data streams  $N_s = 2$  data streams to each user over  $K = 64$  subcarriers with  $N_t = 256$  antennas at BS side and  $N_r = 16$  antennas at each user side. To exhibit the multiuser interference in the wideband multiuser MIMO-OFDM system, all the schemes in this subsection are assumed to have true-time-delay compensation. The optimal digital precoder in the multiuser system is with BD to cancel inter-user interference effect. The one-tier precoder is the Rotman lens-based hybrid precoder without BD operation. We evaluate these schemes under the worse situation with minimum numbers of RF chains, i.e.,  $N_{\text{RF}}^t = UN_s$  and  $N_{\text{RF}}^r = N_s$ .

First, we show the spectral efficiency of different precoding schemes in multiuser mmWave MIMO-OFDM systems with  $U = 4$  users in Fig. 6. It observed that, with the BD operation, the proposed two-tier hybrid precoder could approximate to the optimal digital precoder in the multiuser MIMO-OFDM system. The BD baseband precoder in the first tier could cancel the inter-user interference in multiuser multicarrier system. On the contrary, the spectral efficiency achieved by one-tier precoder is degraded by the residual inter-user interference due to the lack of the BD operation. As shown in Fig. 6, a distinct loss is observed between the one-tier precoder with the other schemes, especially at the high SNR region. The gap

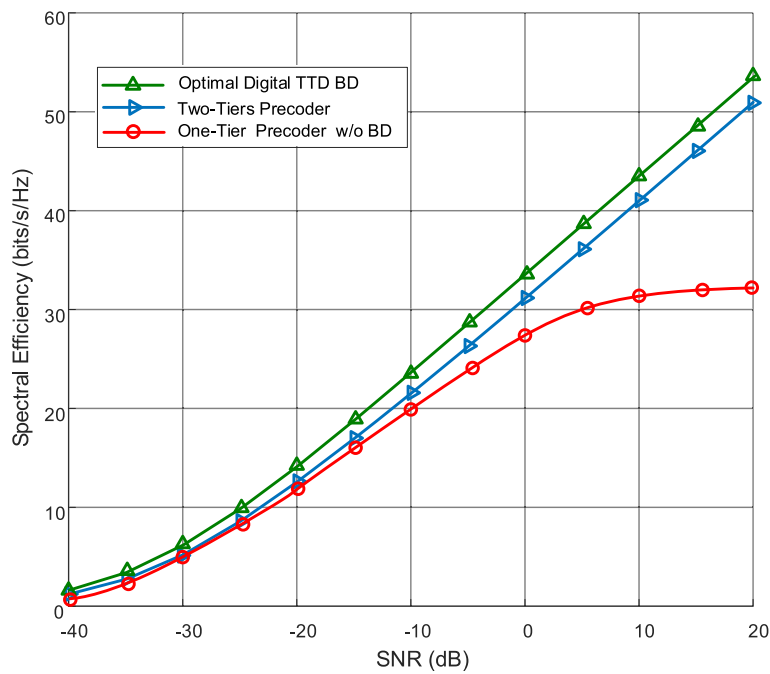


**Fig. 6** Spectral efficiency achieved by different precoding schemes in multiuser mmWave MIMO-OFDM systems with  $U = 4$  users,  $N_t = 256$ ,  $N_r = 16$ , total bandwidth  $B = 1.2$  GHz,  $f_c = 60$  GHz,  $N_{RF}^t = UN_s$ ,  $N_{RF}^r = N_s$

will be even widened with the larger number of subcarriers and users. Therefore, we conclude that, constrained by the degree of the freedom, achieving the hybrid precoder by simply operate matrix factorization to digital precoder is not the optimal results in multiuser multicarrier MIMO systems.

To further illustrate the inter-user interference effect, we evaluate the spectral efficiency of different precoding schemes versus the number of users  $U$  in multiuser mmWave MIMO-OFDM systems under  $SNR = -15$  dB in Fig. 7. With BD operation, the spectral efficiency proposed schemes and optimal digital precoder scheme

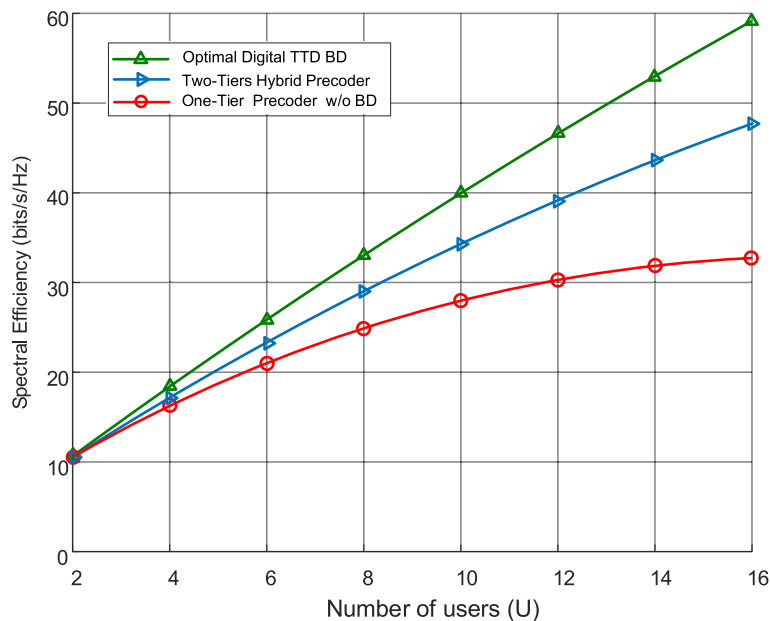


**Fig. 7** Spectral efficiency achieved by different precoding schemes versus the number of users in multiuser mmWave MIMO-OFDM systems under  $SNR = -15$  dB,  $N_t = 256$ ,  $N_r = 16$ , total bandwidth  $B = 1.2$  GHz,  $f_c = 60$  GHz,  $N_{RF}^t = UN_s$ ,  $N_{RF}^r = N_s$

increase with the number of the users. However, the residual inter-user interference is more severe with a larger number of users in the system, and thus degrade the performance. It is observed in Fig. 7 that the spectral efficiency of one-tier precoder is almost saturated when the number of users  $U > 12$ . To summarize, the inter-user interference cancellation techniques are needed for the hybrid structure in the multiuser multicarrier system.

## 6 Conclusion

In this paper, we investigated the hybrid beamforming for the wideband mmWave multiuser MIMO-OFDM system. First, we characterized the beam squint effect in the wideband mmWave channel model. It is verified that both the frequency selectivity and beam squint effect should be considered in the wideband mmWave system. With these observations, we proposed Rotman lens -based two-tier hybrid precoder, aiming to maximize the spectral efficiency. In the first tier, the Rotman lens array-based TTD beamformer was designed to provide true-time-delay and thus reduced the beam squint impairment. Considering the multiuser interference, the first-tier baseband precoder was designed based on block diagonalization in the multiuser system. We considered the finite spatial resolution problem of practical lens array and designed the second-tier hybrid precoder. It could collect the power leakage with much fewer RF chains than full-digital architecture. For future work, we attempt to extend our work in this paper with some other existing wireless techniques [49, 50] and design hybrid precoder for the wideband mmWave system with cache techniques [6–8] to meet the uRLLC requirement in the 5G/B5G communication system.

## Appendix A

Following [18], we demonstrate that semi-orthogonal property of baseband precoder could enable  $\mathbf{F}_{\text{RF}}$  to remove the product form with  $\mathbf{F}_{\text{BB}}$ , which forms the optimization problem (26). With the semi-orthogonal property, the objective function in (24) is rewritten as [18]

$$\begin{aligned} & \|\mathbf{F}_{\text{opt}} - \mathbf{F}_{\text{RF}}\mathbf{F}_{\text{BB}}\|_F^2 \\ &= \text{Tr}(\mathbf{F}_{\text{opt}}^H\mathbf{F}_{\text{opt}}) - \text{Tr}(\mathbf{F}_{\text{opt}}^H\mathbf{F}_{\text{RF}}\mathbf{F}_{\text{BB}}) \\ & \quad - \text{Tr}(\mathbf{F}_{\text{BB}}^H\mathbf{F}_{\text{RF}}^H\mathbf{F}_{\text{opt}}) + \text{Tr}(\mathbf{F}_{\text{BB}}^H\mathbf{F}_{\text{RF}}^H\mathbf{F}_{\text{RF}}\mathbf{F}_{\text{BB}}) \\ &= \|\mathbf{F}_{\text{opt}}\|_F^2 - 2\beta\Re\text{Tr}(\mathbf{G}\mathbf{F}_{\text{opt}}^H\mathbf{F}_{\text{RF}}) + \beta^2\|\mathbf{F}_{\text{RF}}\|_F^2, \end{aligned} \quad (34)$$

where the second equation is by

$$\begin{aligned} & \text{Tr}(\mathbf{F}_{\text{BB}}^H\mathbf{F}_{\text{RF}}^H\mathbf{F}_{\text{RF}}\mathbf{F}_{\text{BB}}) = \beta^2\text{Tr}(\mathbf{G}^H\mathbf{F}_{\text{RF}}^H\mathbf{F}_{\text{RF}}\mathbf{G}) \\ &= \beta^2\text{Tr}(\mathbf{G}\mathbf{G}^H\mathbf{F}_{\text{RF}}^H\mathbf{F}_{\text{RF}}) = \beta^2\text{Tr}(\mathbf{F}_{\text{RF}}^H\mathbf{F}_{\text{RF}}) \\ &= \beta^2\|\mathbf{F}_{\text{RF}}\|_F^2. \end{aligned} \quad (35)$$

The minimum of the objective function is achieved when  $\beta^* = \frac{\Re\text{Tr}(\mathbf{G}\mathbf{F}_{\text{opt}}^H\mathbf{F}_{\text{RF}})}{\|\mathbf{F}_{\text{RF}}\|_F^2}$ . To remove the  $\mathbf{F}_{\text{BB}}$  product from  $\mathbf{F}_{\text{RF}}$ , set  $\beta = 1$ , and we have

$$\begin{aligned} & \|\mathbf{F}_{\text{opt}}\|_F^2 - 2\Re\text{Tr}(\mathbf{G}\mathbf{F}_{\text{opt}}^H\mathbf{F}_{\text{RF}}) + \|\mathbf{F}_{\text{RF}}\|_F^2 \\ &= \text{Tr}(\mathbf{F}_{\text{RF}}^H\mathbf{F}_{\text{RF}}) - 2\Re\text{Tr}(\mathbf{G}\mathbf{F}_{\text{opt}}^H\mathbf{F}_{\text{RF}}) \\ & \quad + \text{Tr}(\mathbf{G}\mathbf{F}_{\text{opt}}^H\mathbf{F}_{\text{opt}}\mathbf{G}^H) \\ &= \|\mathbf{F}_{\text{opt}}\mathbf{G}^H - \mathbf{F}_{\text{RF}}\|_F^2, \end{aligned} \quad (36)$$

which forms the objective function in (26).

## Abbreviations

5G: Fifth generation; AoA: Azimuth angle of arrival and departure; AoD: Azimuth angle of departure; B5G: Beyond-5G; BD : Block diagonalization; DFT: Discrete Fourier transform; MIMO: Multiple-input multiple-output; mmWave: Millimeter wave; OFDM: Orthogonal frequency division multiplexing; OMP: Orthogonal matching pursuit; RF: Radio frequency; TTD: True-time-delay; ULA: Uniform linear array; uRLLC: Ultra-reliable-and-available low-latency communications

## Acknowledgments

Part of this paper was presented in the 29th Annual IEEE International Symposium on Personal, Indoor and Mobile Radio Communications (PIMRC), Bologna, Italy, September 2018 [1].

## Funding

The work of B. Liu, and H. Zhu was supported in part by the National Natural Science Foundation of China under Grant 61427801 and Grant 61871446, and in part by the Postgraduate Research and Practice Innovation Program of Jiangsu Province under Grant KYCX18\_0893.

## Availability of data and materials

The authors confirm that the data supporting the findings of this study are available within the article. All the simulation parameters and other experimental details are clearly shown in this manuscript, which could be used to interpret and replicate the findings reported in the article.

## Authors' contributions

BL conceived and designed the methods. BL performed the experiments and completed the manuscript. HZ gave valuable suggestions on the structure of the paper. Both authors read and approved the final manuscript.

## Competing interests

The authors declare that they have no competing interests.

## Publisher's Note

Springer Nature remains neutral with regard to jurisdictional claims in published maps and institutional affiliations.

## Author details

<sup>1</sup>Jiangsu Key Laboratory of Wireless Communications, Nanjing University of Posts and Telecommunications, 210003 Nanjing, People's Republic of China. <sup>2</sup>Global Big Data Technologies Center, University of Technology Sydney, NSW 2007 Sydney, Australia.

Received: 15 June 2018 Accepted: 31 October 2018

Published online: 22 November 2018

## References

1. B. Liu, W. Tan, H. Hu, H. Zhu, in *Proc. IEEE Annu. Int. Symp. Pers., Indoor, Mobile Radio Commun. (PIMRC)*. Hybrid beamforming for mmWave MIMO-OFDM system with beam squint (IEEE, Bologna, 2018), pp. 1–6
2. J. G. Andrews, S. Buzzi, W. Choi, S. V. Hanly, A. Lozano, A. C. Soong, J. C. Zhang, What will 5g be?. *IEEE J. Sel. Areas Commun.* **32**(6), 1065–1082 (2014)

3. L. Fan, X. Lei, N. Yang, T. Q. Duong, G. K. Karagiannidis, Secrecy cooperative networks with outdated relay selection over correlated fading channels. *IEEE Trans. Veh. Technol.* **66**(8), 7599–7603 (2017)
4. W. Tan, M. Matthaiou, S. Jin, L. Fan, G. K. Karagiannidis, On the Spectral Efficiency of Massive MIMO Systems with Hybrid DFT Processing. *IEEE Trans. Wirel. Commun.* **1**(1), 1–13 (2018)
5. L. Fan, R. Zhao, F.-K. Gong, N. Yang, G. K. Karagiannidis, Secure multiple amplify-and-forward relaying over correlated fading channels. *IEEE Trans. Commun.* **65**(7), 2811–2820 (2017)
6. F. Shi, L. Fan, X. Liu, Z. Na, Y. Liu, Probabilistic caching placement in the presence of multiple eavesdroppers. *Wirel. Commun. Mob. Comput.* **2018**, 1–10 (2018)
7. X. Lai, J. Xia, M. Tang, H. Zhang, J. Zhao, Cache-aided multiuser cognitive relay networks with outdated channel state information. *IEEE Access.* **6**, 21879–21887 (2018)
8. J. Xia, F. Zhou, X. Lai, H. Zhang, H. Chen, Q. Yang, X. Liu, J. Zhao, Cache aided decode-and-forward relaying networks: From the spatial view. *Wirel. Commun. Mobile Comput.* **2018**, 1–9 (2018)
9. W. Tan, M. Matthaiou, S. Jin, X. Li, Spectral efficiency of DFT-based processing hybrid architectures in massive MIMO. *IEEE Wirel. Commun. Lett.* **6**(5), 586–589 (2017)
10. B. Liu, Q. Zhu, W. Tan, H. Zhu, Congestion-optimal WiFi offloading with user mobility management in smart communications. *Wirel. Commun. Mobile Comput.* **2018**, 1–15 (2018)
11. M. Zhang, W. Tan, J. Gao, S. Jin, Spectral efficiency and power allocation for mixed-ADC massive MIMO system. *China Commun.* **15**, 112–127 (2018)
12. Z. Shi, S. Ma, G. Yang, K.-W. Tam, M. Xia, Asymptotic outage analysis of HARQ-IR over time-correlated Nakagami- $m$  fading channels. *IEEE Trans. Commun.* **16**(9), 6119–6134 (2017)
13. L. Fan, N. Zhao, X. Lei, Q. Chen, N. Yang, G. K. Karagiannidis, Outage Probability and Optimal Cache Placement for Multiple Amplify-and-Forward Relay Networks. *IEEE Trans. Veh. Technol.* 1–6 (2019)
14. A. Wiesel, Y. C. Eldar, S. Shamai, Zero-forcing precoding and generalized inverses. *IEEE Trans. Sig. Process.* **56**(9), 4409–4418 (2008)
15. W. Tan, J. Xia, D. Xie, L. Fan, S. Jin, Spectral and energy efficiency of massive MIMO for hybrid architectures based on phase shifters. *IEEE Access.* **6**, 11751–11759 (2018)
16. O. El Ayach, S. Rajagopal, S. Abu-Surra, Z. Pi, R. W. Heath, Spatially sparse precoding in millimeter wave MIMO systems. *IEEE Trans. Wirel. Commun.* **13**(3), 1499–1513 (2014)
17. C. Li, S. Zhang, P. Liu, F. Sun, J. M. Cioffi, L. Yang, Overhearing protocol design exploiting intercell interference in cooperative green networks. *IEEE Trans. Veh. Technol.* **65**(1), 441–446 (2016)
18. X. Yu, J.-C. Shen, J. Zhang, K. B. Letaief, Alternating minimization algorithms for hybrid precoding in millimeter wave MIMO systems. *IEEE Sel. J. Top. Sign. Process.* **10**(3), 485–500 (2016)
19. F. Sohrabi, W. Yu, Hybrid digital and analog beamforming design for large-scale antenna arrays. *IEEE Sel. J. Top. Sign. Process.* **10**(3), 501–513 (2016)
20. D. H. N. Nguyen, L. B. Le, T. Le-Ngoc, in *Proc. IEEE Int. Conf. Commun. (ICC)*. Hybrid MMSE precoding for mmwave multiuser MIMO systems (IEEE, Kuala Lumpur, 2016), pp. 1–6
21. X. Yu, J. Zhang, K. B. Letaief, in *Proc. Asilomar Conf. Signals Syst. Comput.* Alternating minimization for hybrid precoding in multiuser OFDM mmwave systems (IEEE, Pacific Grove, 2016), pp. 281–285
22. A. Alkhateeb, R. W. Heath, Frequency selective hybrid precoding for limited feedback millimeter wave systems. *IEEE Trans. Commun.* **64**(5), 1801–1818 (2016)
23. F. Sohrabi, W. Yu, Hybrid analog and digital beamforming for mmWave OFDM large-scale antenna arrays. *IEEE Sel. J. Areas Commun.* **35**(7), 1432–1443 (2017)
24. S. Park, A. Alkhateeb, R. W. Heath, Dynamic subarrays for hybrid precoding in wideband mmWave MIMO systems. *IEEE Trans. Wirel. Commun.* **16**(5), 2907–2920 (2017)
25. R. Peng, Y. Tian, in *Proc. IEEE Int. Workshop Signal Process. Adv. Wireless Commun. (SPAWC)*. Wideband hybrid precoder design in MU-MIMO based on channel angular information (IEEE, Sapporo, 2017), pp. 1–5
26. M. Cai, J. N. Laneman, B. Hochwald, in *Proc. IEEE Int. Symp. Inf. Theory (ISIT)*. Beamforming codebook compensation for beam squint with channel capacity constraint (IEEE, Aachen, 2017), pp. 76–80
27. B. Wang, F. Gao, S. Jin, H. Lin, G. Y. Li, Spatial- and frequency-wideband effects in millimeter-wave massive MIMO systems. *IEEE Trans. Sign. Process.* **66**(13), 3393–3406 (2018)
28. S. M. Perera, V. Ariyaratna, N. Udayanga, A. Madanayake, G. Wu, L. Belostotski, Y. Wang, S. Mandal, R. J. Cintra, T. S. Rappaport, Wideband N-beam arrays using low-complexity algorithms and mixed-signal integrated circuits. *IEEE Sel. J. Top. Sign. Process.* **12**(2), 368–382 (2018)
29. W. Tan, X. Li, D. Xie, L. Fan, S. Jin, On the performance of three dimensional antenna arrays in millimeter wave propagation environments. *IET Commun.* **12**(17), 1743–1750 (2018)
30. W. Tan, S. Jin, C.-K. Wen, T. Jiang, Spectral efficiency of multi-user millimeter wave systems under single path with uniform rectangular arrays. *EURASIP Wirel. J. Commun. Netw.* **181**, 458–472 (2017)
31. M. Cai, K. Gao, D. Nie, B. Hochwald, J. N. Laneman, H. Huang, K. Liu, in *Proc. IEEE Global Commun. Conf. (GLOBECOM)*. Effect of wideband beam squint on codebook design in phased-array wireless systems (IEEE, Washington, 2016), pp. 1–6
32. M. Cai, J. N. Laneman, B. Hochwald, in *Proc. IEEE Global Commun. Conf. (GLOBECOM)*. Carrier aggregation for phased-array analog beamforming with beam squint (IEEE, Singapore, 2017), pp. 1–7
33. W. Tan, G. Xu, E. D. Carvalho, et al., Low cost and high efficiency hybrid architecture massive MIMO systems based on DFT processing. *Wireless Commun. Mob. Comput.* **2018**, 1–11 (2018)
34. J. Li, X. Jiang, Y. Yan, W. Yu, S. Song, M. H. Lee, Low complexity detection for quadrature spatial modulation systems. *Wirel. Pers. Commun.* **95**(4), 4171–4183 (2017)
35. C. Li, K. Song, Y. Li, L. Yang, Energy efficient design for multiuser downlink energy and uplink information transfer in 5G. *Science China Information Sciences.* **59**(2) (2016)
36. R. Zhao, Y. Yuan, L. Fan, Y.-C. He, Secrecy performance analysis of cognitive decode-and-forward relay networks in Nakagami- $m$  fading channels. *IEEE Trans. Commun.* **65**(2), 549–563 (2017)
37. C. Li, K. Song, D. Wang, F.-C. Zheng, L. Yang, Optimal remote radio head selection for cloud radio access networks. *Sci. China Inf. Sci.* **59**(10), 2016
38. Y. Gao, M. Khalil, F. Zheng, T. Kaiser, Rotman lens based hybrid analog-digital beamforming in massive MIMO systems: Array architectures, beam selection algorithms and experiments. *IEEE Trans. Veh. Technol.* **66**(10), 9134–9148 (2017)
39. R. Rotman, M. Tur, L. Yaron, True time delay in phased arrays. *IEEE Proc.* **104**(3), 504–518 (2016)
40. T. Xie, L. Dai, X. Gao, H. Yao, X. Wang, in *Proc. IEEE Veh. Technol. Conf. (VTC-Fall)*. On the power leakage problem in beamspace MIMO systems with lens antenna array (IEEE, Toronto, 2017), pp. 1–5
41. Z. Na, Y. Wang, X. Li, J. Xia, et al., Subcarrier allocation based simultaneous wireless information and power transfer algorithm in 5G cooperative OFDM communication systems. *Phys. Commun.* **29**, 164–170 (2018)
42. M. Zhao, D. Deng, W. Zhou, L. Fan, Non-renewable energy efficiency optimization in energy harvesting relay-assisted system. *Phys. Commun.* **28**, 183–190 (2018)
43. C. Li, Y. Li, K. Song, L. Yang, Energy efficient design for multiuser downlink energy and uplink information transfer in 5G. *Sci. China Inf. Sci.* **59**(2), 1–8 (2016)
44. X. Lai, W. Zou, X. Li, L. Fan, Multiuser energy harvesting relaying system with direct links. *IET Commun.* **11**(12), 1846–1852 (2017)
45. F. Zhou, L. Fan, X. Lei, G. Luo, H. Zhang, J. Zhao, Edge caching with transmission schedule for multiuser multirelay networks. *IEEE Commun. Lett.* **22**(4), 776–779 (2018)
46. X. Yu, J. Zhang, K. B. Letaief, A hardware-efficient analog network structure for hybrid precoding in millimeter wave systems. *IEEE Sel. J. Top. Sign. Process.* **12**(2), 282–297 (2018)
47. L. Fan, X. Lei, N. Yang, T. Q. Duong, G. K. Karagiannidis, Secure multiple amplify-and-forward relaying with cochannel interference. *IEEE Sel. J. Top. Sign. Process.* **10**(8), 1494–1505 (2016)
48. Q. H. Spencer, A. L. Swindlehurst, M. Haardt, Zero-forcing methods for downlink spatial multiplexing in multiuser MIMO channels. *IEEE Trans. Sign. Process.* **52**(2), 461–471 (2004)
49. Z. Song, Z. Zhang, X. Liu, Y. Liu, L. Fan, Simultaneous cooperative spectrum sensing and wireless power transfer in multi-antenna cognitive radio. *Phys. Commun.* **29**, 78–85 (2018)
50. X. Liu, X. Zhang, M. Jia, L. Fan, et al., 5G-based green broadband communication system design with simultaneous wireless information and power transfer. *Phys. Commun.* **28**, 130–137 (2018)